Supporting Information

Synergistic Crystalline Catalysts Assembled with Wells-Dawson-type Polyoxometalate and Heterovalent Metal-Complex for Efficient Benzylic C-H Bond Oxidation

Ze-Xuan Liu, Jing Du, Shuai Li, Miao-Qi Zhu, Yuan-Yuan Ma,* Zhan-Gang Han**

Hebei Technology Innovation Center for Energy Conversion Materials and Devices, National Demonstration Center for Experimental Chemistry Education, Testing and Analysis Center, College of Chemistry and Materials Science,

Hebei Normal University, Shijiazhuang, Hebei 050024, P. R. China

Email: duj622@hebtu.edu.cn; mayy334@hebtu.edu.cn; hanzg116@126.com; hanzg116@hebtu.edu.cn

CONTENTS:

1. Supplementary Experimental Section

1.1 Materials and measurements.

The Dawson-type POM anion was synthesized according to the previous literature methods.[1] All others chemicals and reagents used in this study were commercially purchased from the supplier and used without further purification. Fourier transform infrared (FTIR) spectra were recorded on a Thermo SCIENTIFIC apparatus. C, H and N elemental analyses were performed by Perkin-Elmer 2400 elemental analyzer; P, W, Cu, Cl were acquired using a Prodigy XP emission spectrometer. The powder X-ray diffraction (XRD) patterns were recorded on a Smart Lab X-Ray diffractometer with Cu-Kα (λ = 1.5418 Å) radiation in the 2θ range from 5° to 50° at a scanning rate of 2° per minute. Thermogravimetric analyses (TGA) were performed on a SDT Q600 TG instrument heated from room temperature to 800 °C with a heating rate of 10 °C·min^{-1}, under a dynamic nitrogen atmosphere. Gas chromatography (GC) analysis was performed on an Agilent Technologies 7890B gas chromatography system with nitrogen as the carrier gas. Electron paramagnetic resonance (EPR) was analyzed by Magnettech MS-5000. X-ray photoelectron spectroscopy (XPS) was tested on the ESCALAB QXi X-ray energy spectrometer.

1.2 X-ray crystallography.

Single crystals of compounds **1**, **2** and [Cu_3DTAB]Cl_3 with regular shape were collected under optical microscope. The crystallographic data were collected on a XtaLAB Synergy, Dualflex, HyPix diffractometer with Cu Kα radiation (λ = 1.54056 Å) and Mo Kα radiation (λ = 0.71073 Å) at the temperature of 298(2) K. Compounds **1**, **2** and

$[Cu_3DTAB]Cl_3$ were kept at 293(2) K during data collection. Using Olex2,[2] the structure was solved with the olex2.solve[3] structure solution program using Charge Flipping and refined with the XL[4] refinement package using Least Squares minimisation. Crystallographic data and structural refinements details of compound **1**, **2** and $[Cu_3DTAB]Cl_3$ are provided in Table S1 and Table S8. The selected bond distances (Å) and angles (°) for compound **1**, **2** and $[Cu_3DTAB]Cl_3$ are given in Tables S2, S3 and S9. The CCDC reference numbers for compound **1**, **2** and $[Cu_3DTAB]Cl_3$ are 2400900, 2400907, 2400908, respectively.

1.3 Selective Catalytic Oxidation of Benzyl C-H bonds

At room temperature, DPM (0.3 mmol), catalyst (0.007 mmol), acetonitrile (3 mL) and TBHP (4.95 mmol) were successively added to a 10 mL glass reactor. The reactor was placed in a water-bath equipped with a magnetic stirrer and temperature control, and reacted at 80 °C. During the reaction, a certain amount of reaction solution was taken out regularly for centrifugation. The obtained filtrate was analyzed by Gas chromatography (GC) analysis to determine the conversion and selectivity. After the end of the reaction, the catalysts were washed by using acetonitrile and vacuum dried at 100 °C for 24 h to be reused in the cycle experiment.

1.4 EPR measurement

The details of the EPR experiments were as follows: TBHP (4.95 mmol) and compound **1** (0.007 mmol) were mixed in acetonitrile (3 mL). The selected spin traps, N-tert-butyl-α-phenylnitrone (PBN) and 5,5-dimethyl-1-pyrroline-N-oxide (DMPO), were added to

the above solution and stirred for 10 minutes to detect the signals of active radicals, including the PBN/•OBu^t spin adduct and hydroxyl radicals (•OH).

1.5 The experiment for scavenging radicals

Under the optimal reaction conditions, Butylated hydroxytoluene (BHT) (4.95 mmol) was added to the reaction system as an oxygen radical scavenger. After 8 hours, a certain amount of the reaction mixture was withdrawn and processed by centrifugation. Under the optimal reaction conditions, Isopropanol (IPA) (3 mmol) was added to the reaction system as •OH radical scavenger. After 8 hours, a certain amount of the reaction mixture was withdrawn and processed by centrifugation. Subsequently, the aforementioned filtrate was analyzed by gas chromatography (GC) to determine the conversion rate and selectivity.

1.6 Computational Methods

All calculations were performed using the Gaussian program package with D1 version[5] at PBE1PBE-D3 level without symmetry restrictions.[6-8] Basis sets with LANL2DZ and 6-31G(d,p) were used for metal atoms (W and Cu) and nonmetal atoms (H, O, C, N and P), respectively.[9] In all steps, the solvation effects were introduced to mimic an aqueous solution by using the PCM model.[10]

II. Supplementary Structure Figure.

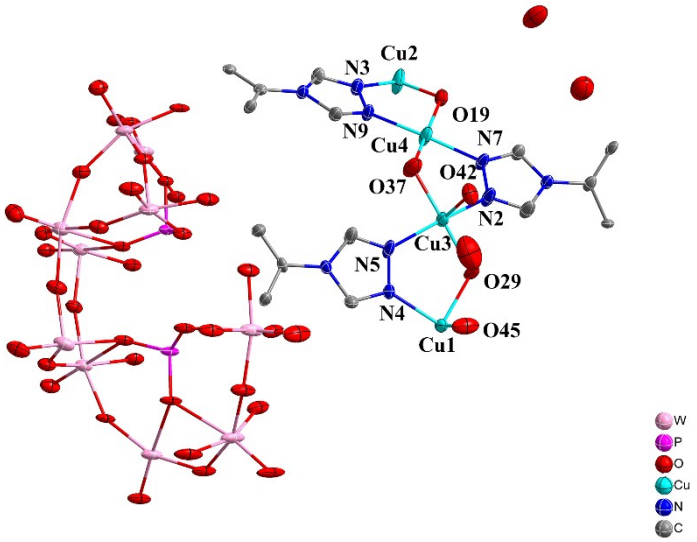

Figure S1. The asymmetric unit of compound **1** with thermal ellipsoids at 30% probability displacement.

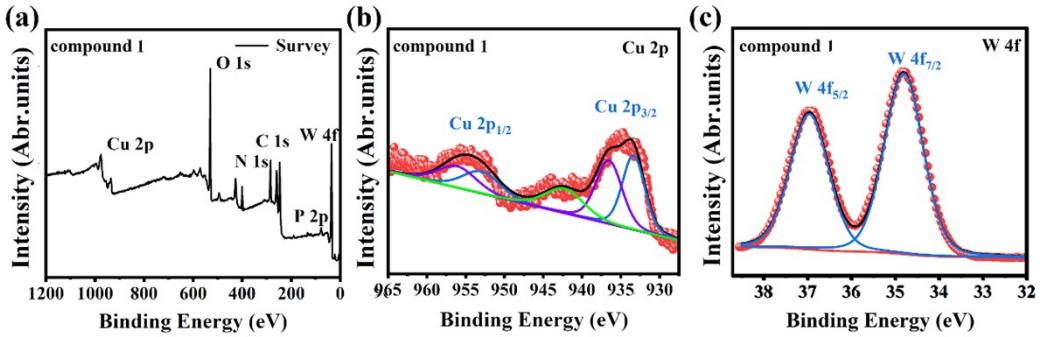

Figure S2. (a) XPS survey, (b) Cu 2p and (c) W 4f high-resolution XPS spectra of compound **1**.

In the full XPS spectrum of compound **1**, the characteristic peaks of Cu, N, C, P, W, and O can be clearly observed. The high-resolution XPS spectrum of W 4f in compound **1** shows two characteristic peaks at 34.8 eV and 36.9 eV, which correspond to the characteristic absorption of W^{VI} $4f_{7/2}$ and W^{VI} $4f_{5/2}$, respectively.[11] The high resolution

XPS spectra of Cu 2p showed the peaks centered at 933.3 and 953.1 eV correspond to the signals of Cu^{I} $2p_{3/2}$ and Cu^{I} $2p_{1/2}$. The binding energies located at 936.5 and 956.3 eV are assigned to Cu^{II} $2p_{3/2}$ and Cu^{II} $2p_{1/2}$.[12] The peak areas of the Cu^{I} and Cu^{II} signals are in the ratio of 1:1, which is consistent with the molecular formula.

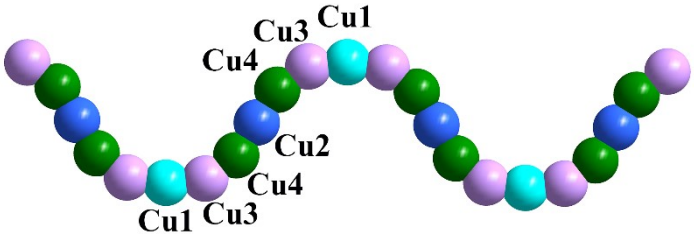

Figure S3. The repeating monomer $[Cu_3^{I}Cu_3^{II}(\mu_2\text{-}OH)_6(H_2O)_3]^{3+}$ of compound **1**

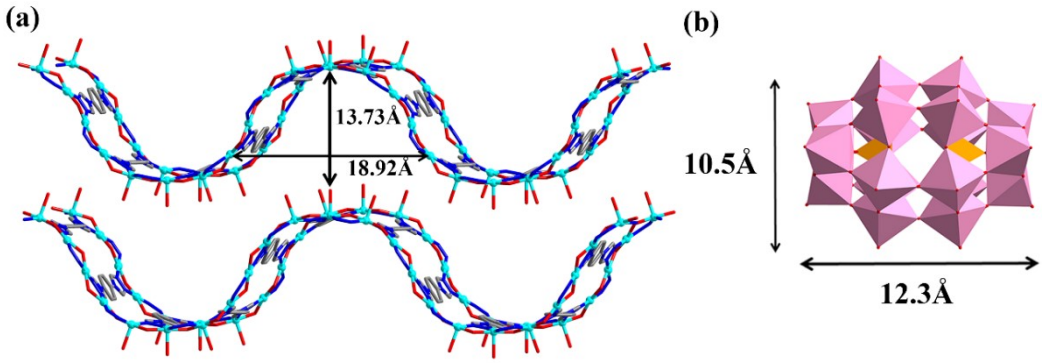

Figure S4. (a) The size of cavity produced by the parallel stacking of 2-D metal-organic cation networks along the *b*-axis in compound **1**. (b) The size of $[P_2W_{18}O_{62}]^{6-}$ anion.

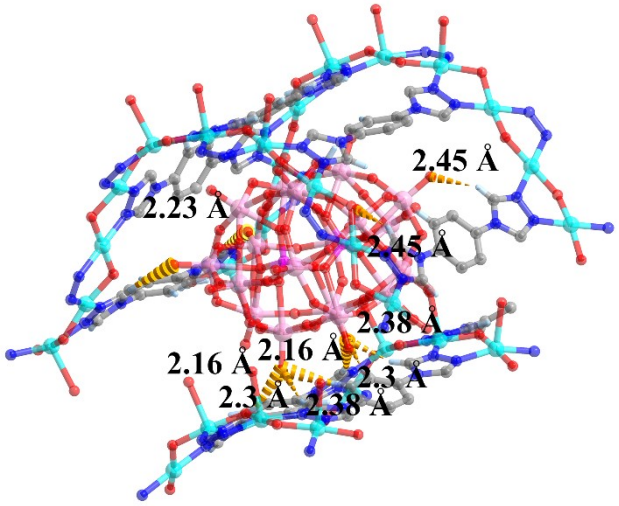

Figure S5. Hydrogen bonding interactions between Cu-organic fragment and $[P_2W_{18}O_{62}]^{6-}$ anion in compound **1**.

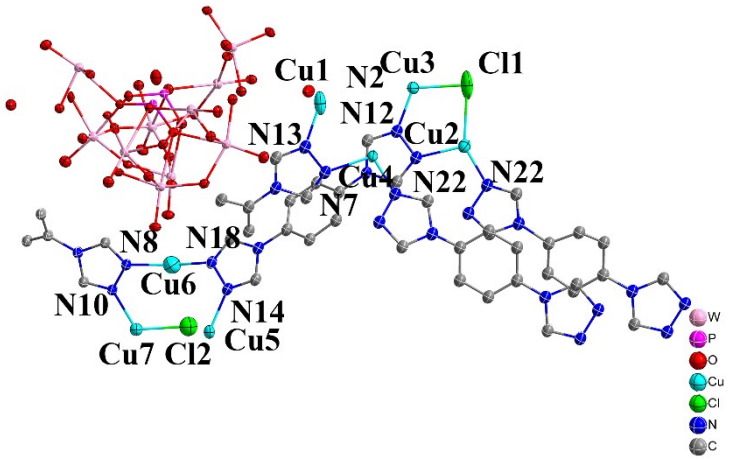

Figure S6. The asymmetric unit of compound **2** with thermal ellipsoids at 30% probability displacement.

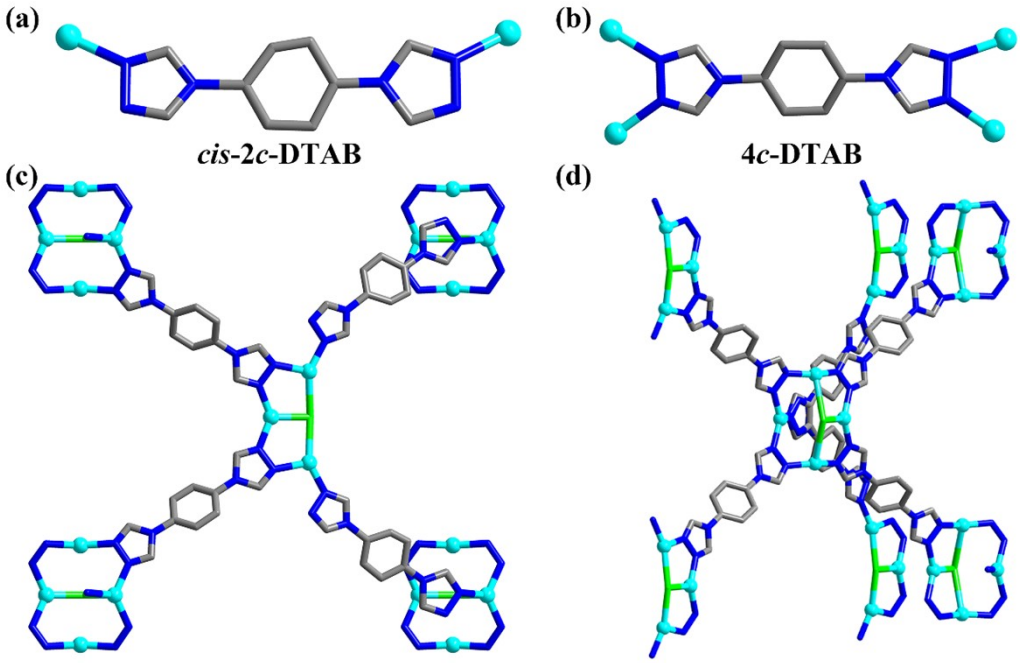

Figure S7. (a) Coordination mode of *cis*-2*c*-DTAB in compound **2**; (b) Coordination mode of 4*c*-DTAB in compound **2;** (c) Coordination mode of $\{Cu_3Cl\}$ unit; (d) Coordination mode of $\{Cu_4Cl\}$ unit in compound **2**.

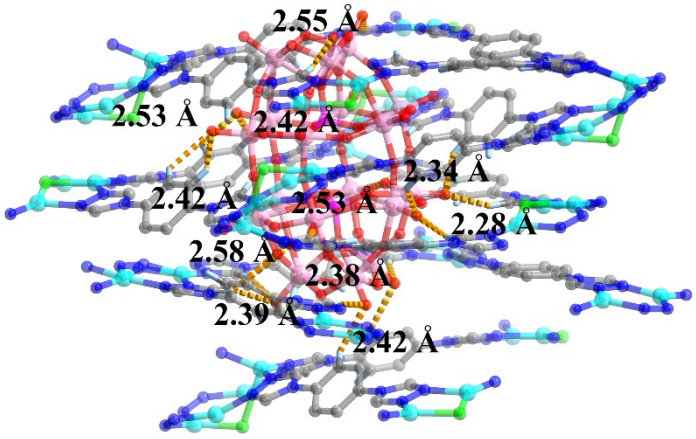

Figure S8. Hydrogen bonding interactions between $[P_2W_{18}O_{62}]^{6-}$ anion and DTAB ligands in compound **2**.

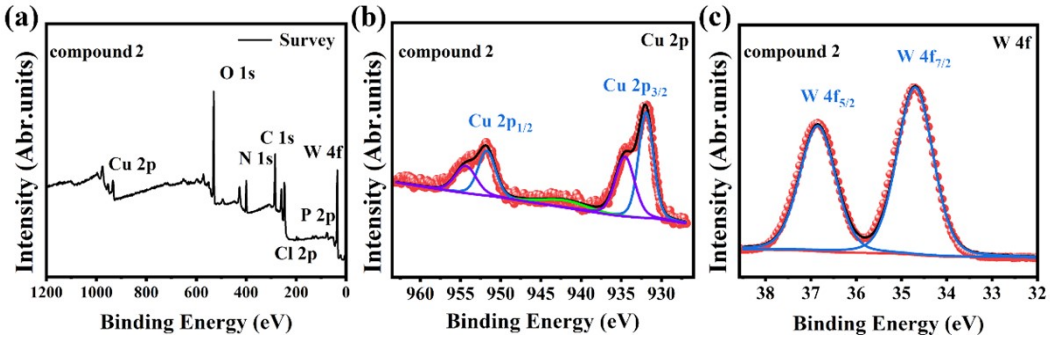

Figure S9. (a) XPS survey, (b) Cu 2p and (c) W 4f high-resolution XPS spectra of compound **2**.

The full XPS spectrum of compound **2** in Figure S9 shows the characteristic peaks of Cu, N, C, P, Cl, W, and O elements. And the high-resolution XPS spectrum of W 4f in compound **2** shows two characteristic peaks at 34.7 eV and 36.8 eV, which correspond to the characteristic absorption of W^{VI} $4f_{7/2}$ and W^{VI} $4f_{5/2}$, respectively.[11] The high resolution XPS spectra of Cu 2p showed the peaks centered at 931.9 and 951.7 eV correspond to the $2p_{3/2}$ and $2p_{1/2}$ signals of Cu^{I} with coordination environment of {CuNNN}, and the other two peaks at 934.5 and 954.3 eV are attributed to the $2p_{3/2}$ and $2p_{1/2}$ signals of Cu^{I} with coordination environment of {CuNNCl}.

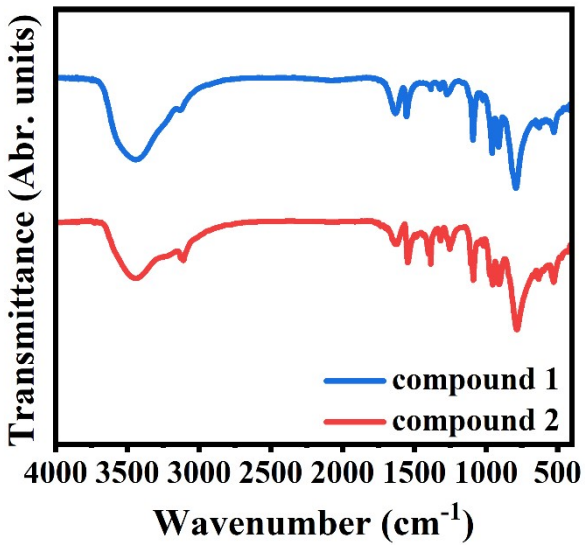

Figure S10. IR spectra of compounds **1–2**.

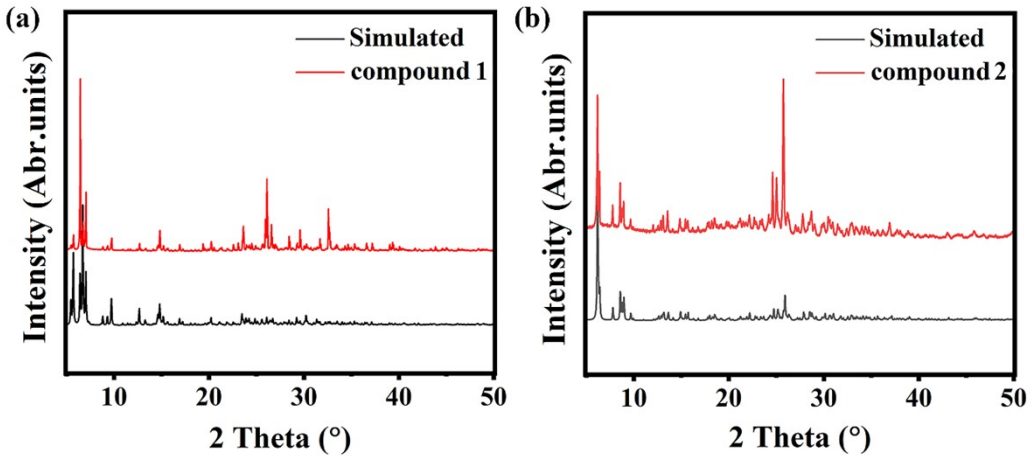

Figure S11. XRD patterns of compounds **1–2**.

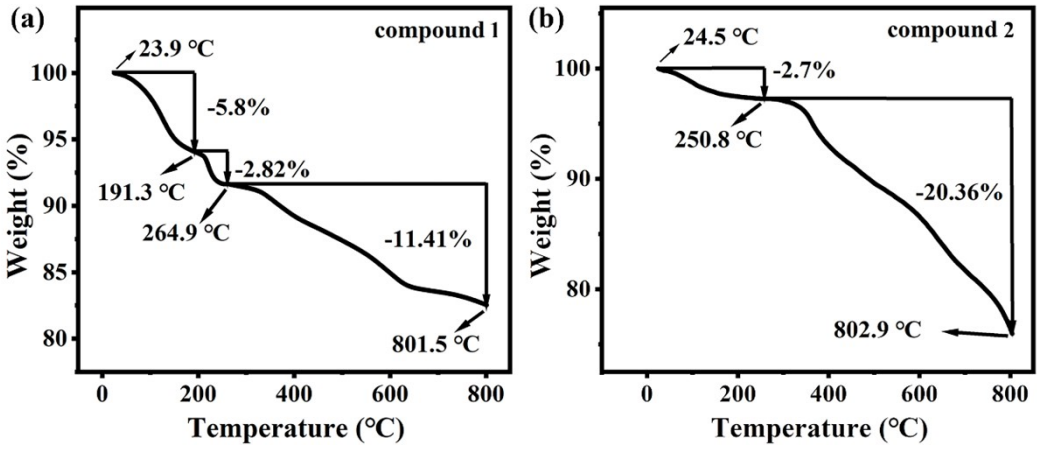

Figure S12. TG curves of compounds **1–2.**

The TG curves of compounds **1-2** were shown in Figure S12. Compound **1** presents three steps of weight loss, which lost 5.8% weight in the temperature range of 23.9–191.3 °C, 2.82% weight in the temperature range of 191.3–264.9 °C, and 11.41% weight in the temperature range of 264.9–801.5 °C. These processes are attributed to the loss of eighteen lattice water molecules (calculated value 5.8%), three coordination water molecules and six hydroxyl groups (calculated value 2.8%), and the decomposition of six ligand (calculated value 11.50%). Compound **2** presents two steps of weight loss, which lost 2.7% weight in the temperature range of 24.5–250.8 °C and 20.36% weight in the temperature range of 250.8–802.9 °C. These processes are attributed to the loss of nine lattice water molecules (calculated value 2.8%) and the decomposition of three ligand (calculated value 11.50%). The main structure of compounds **1** and **2** can be maintained about 265 °C, so these compounds showed good thermal stability, which provided a guarantee for the structural stability of the catalyst in the heterogeneous catalytic system.

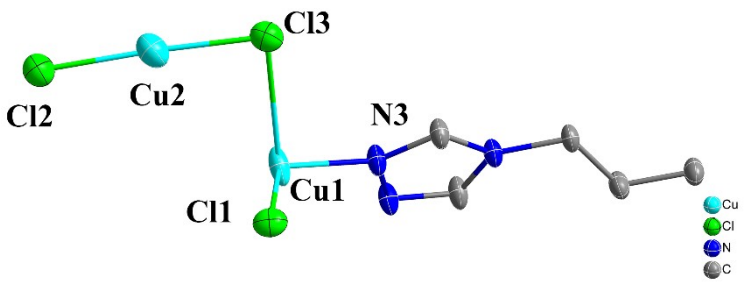

Figure S13. The asymmetric unit of $[Cu_3DTAB]Cl_3$ with thermal ellipsoids at 30% probability displacement.

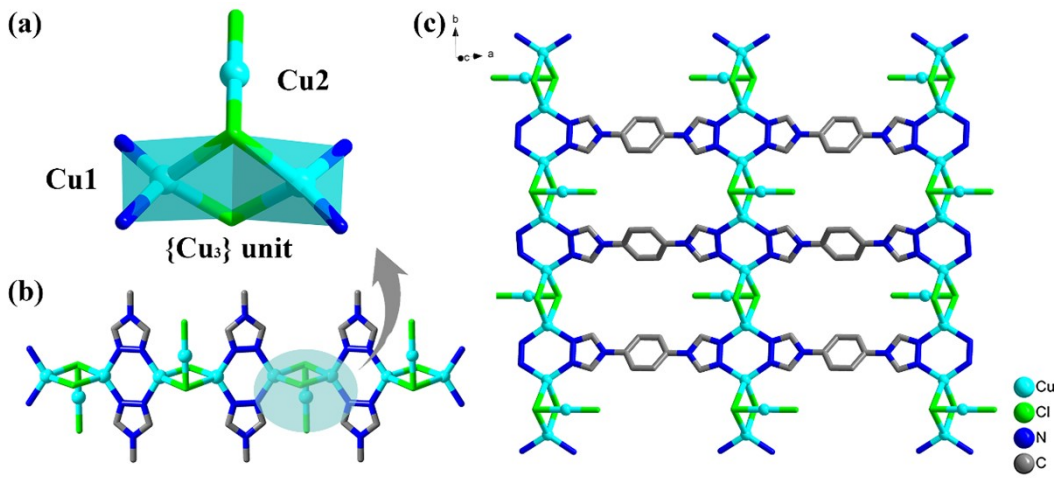

Figure S14. (a) $[Cu^{I}_{3}(\mu_2\text{-}Cl)_2Cl(N\text{–}N)]$ unit in $[Cu_3DTAB]Cl_3$; (b) 1-D metal-organic chain in $[Cu_3DTAB]Cl_3$; (c) 2-D metal-organic network of $[Cu_3DTAB]Cl_3$.

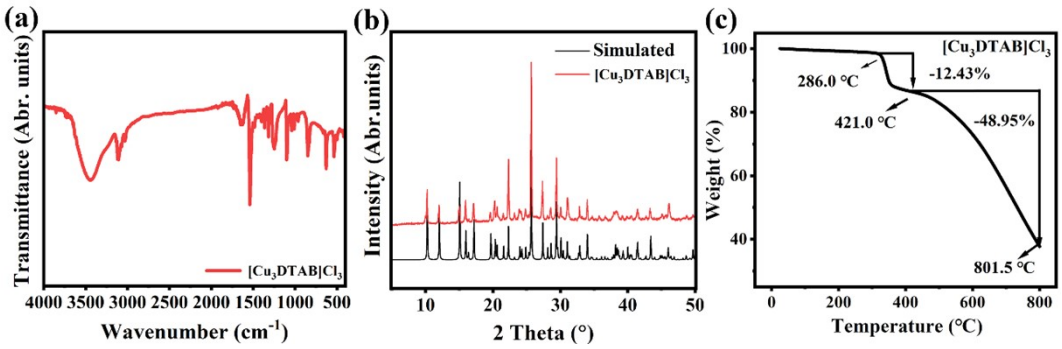

Figure S15. (a) IR spectrum of $[Cu_3DTAB]Cl_3$; (b) XRD patterns of $[Cu_3DTAB]Cl_3$; (c) TG curve of $[Cu_3DTAB]Cl_3$.

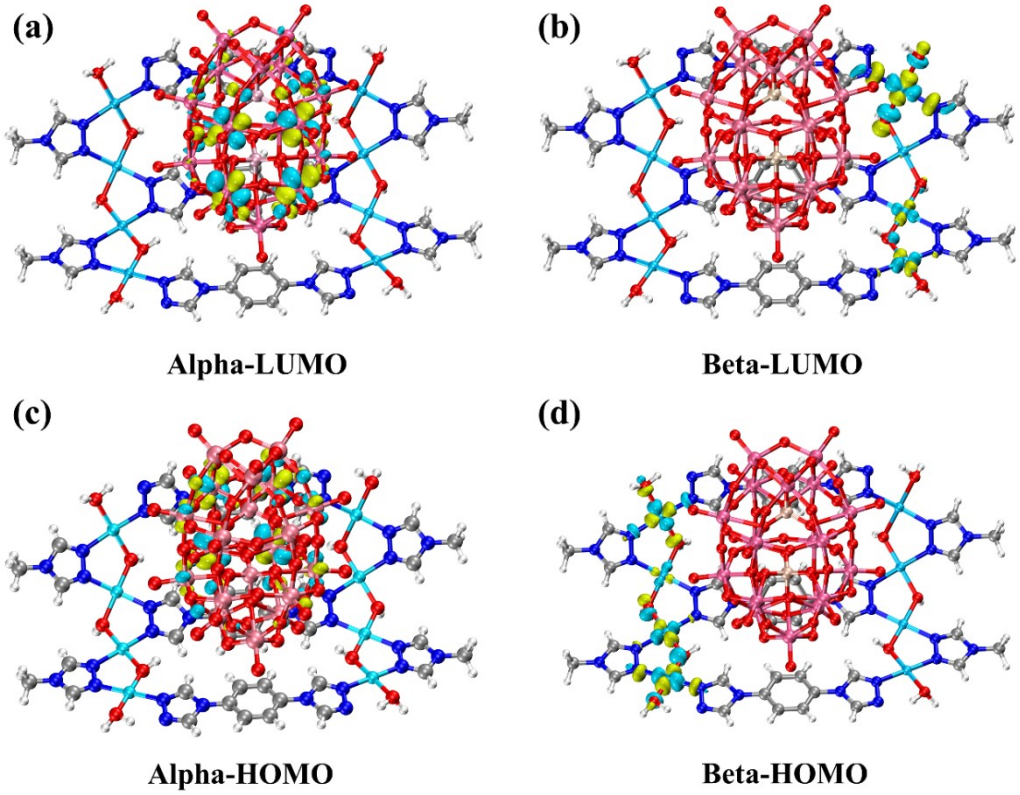

Figure S16. The lowest unoccupied molecular orbital (LUMO) and highest occupied molecular orbital (HOMO) of compound **1**

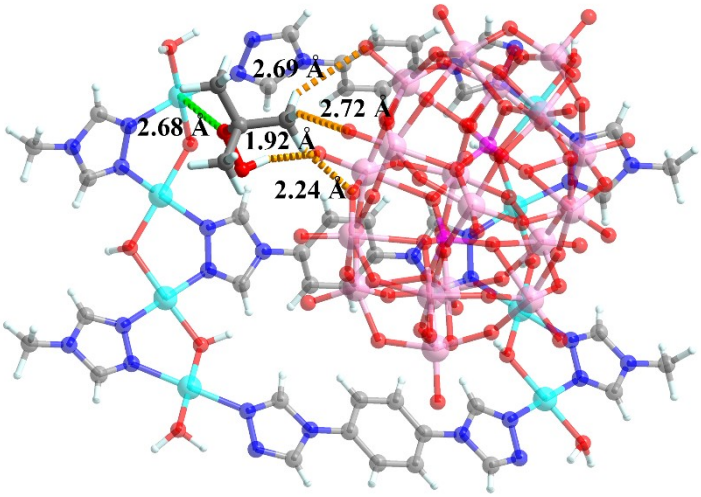

Figure S17. The interactions among *t*-BuOOH, Dawson-type polyoxoanions and Cu sites within compound **1.**

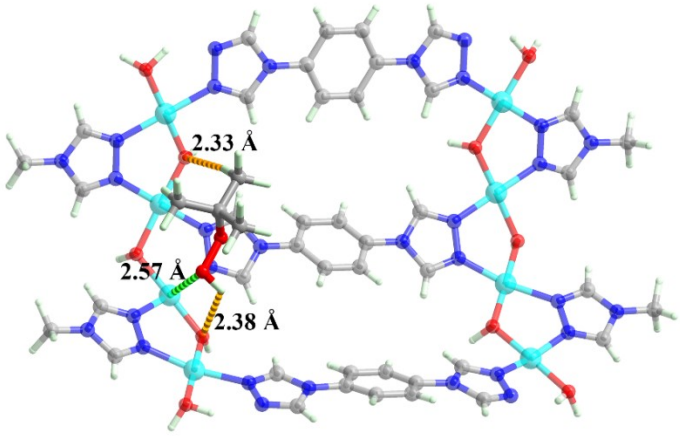

Figure S18. The interactions of *t*-BuOOH with Cu sites and μ_2-O oxygen atoms within Cu-DTAB complex.

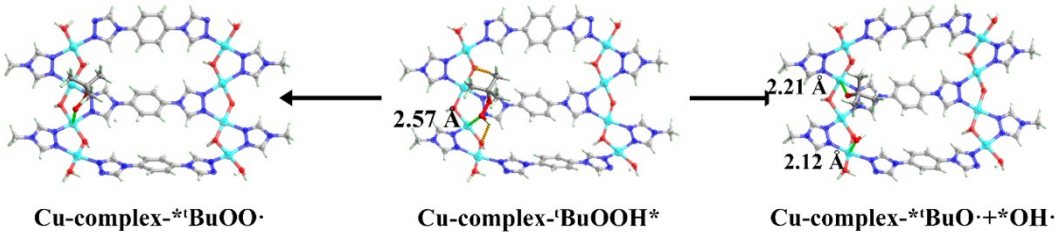

Figure S19. Two pathways of *t*-BuOOH cleavage into carbon-centered radical intermediates (*t*-BuOO• and *t*-BuO•) over Cu-DTAB complex.

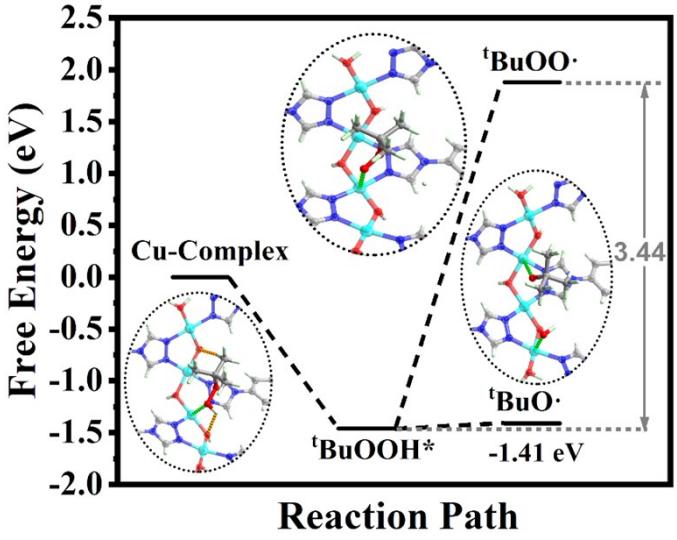

Figure S20. The adsorption energies of the *t*-BuOO• and *t*-BuO• species over Cu-DTAB complex.

Figure S20 illustrates the adsorption energy of the Cu-complex after adsorbing *t*-BuOOH to generate the *t*-BuOO• species or the *t*-BuO• species. Similar to the results with compound **1**, the Cu-complex also requires a higher energy barrier to activate *t*-BuOOH to produce *t*-BuOO• species, indicating that *t*-BuO• is the main active intermediate. The adsorption energy for the formation of *t*-BuO• on the Cu-complex (ΔG = -1.41 eV) is greater than that on compound **1** (ΔG = -1.50 eV), suggesting that the introduction of Dawson-type polyanions into the Cu complex facilitates the formation of the *t*-BuO• species.

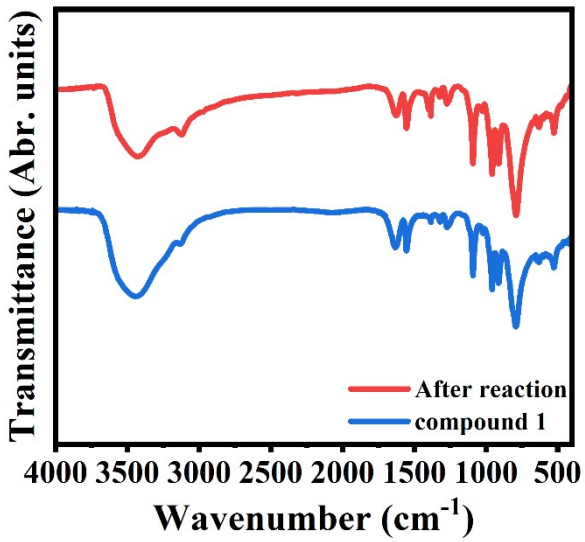

Figure S21. IR spectra of compound **1** before and after catalytic reaction.

3. Supplementary Tables

Table S1. Crystal Data and Structural Refinement Details for compounds 1–2.

Compound	**1**	**2**
Formula	$C_{30}H_{24}Cu_6N_{18}O_{71}P_2W_{18}$	$C_{60}H_{48}Cl_2Cu_8N_{36}O_{65}P_2W_{18}$
Mr	5525.15	6263.80
Crystal system	orthorhombic	monoclinic
Space group	*C*mce	$P2_1/m$
a [Å]	26.3262(2)	14.6284(5)
b [Å]	27.4766(2)	19.7049(6)
c [Å]	30.9255(2)	21.7702(8)
α, β , γ[°]	90, 90, 90	90, 109.011(4), 90
V [Å^3]	22370.1(3)	5933.0(4)
Z	8	2
Density (Mg/m^3)	3.281	3.506
Absorption coefficient (mm^{-1})	35.454	18.943
$F_{(000)}$	19472.0	5616.0
Cryst size(mm^3)	0.11 × 0.11 × 0.07	0.15 × 0.12 × 0.11
θ (deg)	5.458 – 133.196	4.134 – 50.054
Reflections collected	40061	25927
Independent reflections	10004	10415
GOF on F^2	1.052	1.039
Final *R* indices, R_1	0.0469	0.0355
$wR_2[I>2\sigma(I)]$	0.1287	0.0912
R indices, R_1	0.0507	0.0444
wR_2(all data)	0.1314	0.0965

Table S2. Selected bond lengths (Å) and bond angles (°) of compound **1**.

Cu(1)-O(29)	1.934(9)	Cu(1)-N(4)	2.006(9)	Cu(1)-O(45)	2.32(2)
Cu(1)-O(29^{2})	1.934(9)	Cu(1)-N(4^{2})	2.006(9)	Cu(2)-N(3)	2.004(10)
Cu(2)-O(41)	1.906(18)	Cu(2)-O(41^{3})	1.906(17)	Cu(2)-N(3^{2})	2.004(10)
Cu(2)-O(19)	1.929(17)	Cu(3)-O(29)	1.934(9)	Cu(3)-O(37)	1.930(11)
Cu(3)-N(2)	1.984(10)	Cu(3)-N(5)	2.012(11)	Cu(3)-O(42)	2.34(2)
Cu(4)-N(9)	1.983(9)	Cu(4)-N(7)	1.972(9)	Cu(4)-O(41)	1.906(18)
Cu(4)-O(19)	1.941(16)	O(29^{2})-Cu(1)-O(29)	178.1(8)	O(29^{2})-Cu(1)-N(4^{2})	87.5(4)
O(29^{2})-Cu(1)-N(4)	92.7(4)	O(29)-Cu(1)-N(4)	87.5(4)	O(29)-Cu(1)-O(45)	89.1(4)
O(29^{2})-Cu(1)-O(45)	89.1(4)	N(4^{2})-Cu(1)-N(4)	165.8(6)	N(4)-Cu(1)-O(45)	97.1(3)
N(4^{2})-Cu(1)-O(45)	97.1(3)	N(3)-Cu(2)-N(3^{3})	180.0	O(41^{3})-Cu(2)-N(3)	90.6(6)
O(41)-Cu(2)-N(3)	89.4(6)	O(41^{3})-Cu(2)-O(41)	180.0	O(41)-Cu(2)-O(19^{3})	157.0(6)
Cu(3)-O(37)-Cu(4)	116.4(6)	O(19^{3})-Cu(2)-N(3^{3})	86.2(6)	O(19)-Cu(2)-N(3)	86.2(6)
O(19^{3})-Cu(2)-N(3)	93.8(6)	O(19)-Cu(2)-N(3^{3})	93.8(6)	O(19^{3})-Cu(2)-O(19)	180.0
O(29)-Cu(3)-N(2)	91.0(4)	O(29)-Cu(3)-N(5)	87.7(4)	O(29)-Cu(3)-O(42)	92.7(7)
O(37)-Cu(3)-O(29)	175.7(7)	O(37)-Cu(3)-N(2)	88.1(4)	O(37)-Cu(3)-O(42)	91.5(8)
N(2)-Cu(3)-N(5)	158.3(7)	N(2)-Cu(3)-O(42)	96.9(7)	N(5)-Cu(3)-O(42)	104.8(6)
N(7)-Cu(4)-O(37)	87.5(4)	N(7)-Cu(4)-N(9)	178.7(6)	N(9)-Cu(4)-O(37)	93.1(4)
O(41)-Cu(4)-O(37)	167.9(9)	O(41)-Cu(4)-N(7)	89.7(6)	O(41)-Cu(4)-N(9)	89.5(6)
O(19)-Cu(4)-O(37)	169.1(8)	O(19)-Cu(4)-N(7)	92.9(6)	O(19)-Cu(4)-N(9)	86.8(6)
Cu(3)-O(29)-Cu(1)	123.1(5)				

Symmetry transformations used to generate equivalent atoms: ^{1}1-x,+y,+z; ^{2}3/2-x,+y,3/2-z; ^{3}3/2-x,3/2-y,1-z; ^{4}2-x, +y, +z.

Table S3. The hydrogen bond lengths (Å) and angles (°) of compound **1**.

Donor-H···Acceptor	D-H [Å]	H···A [Å]	D···A [Å]	D-H···A [°]
C(5)-H(5)···O(40)	0.93	2.23	3.153(15)	172
C(6)-H(6)···O(36)	0.93	2.30	3.159(15)	154
C(7)-H(7)···O(36)	0.93	2.16	3.054(19)	161
C(10)-H(10)···O(36)	0.93	2.38	3.309(15)	173
C(11)-H(11)···O(40)	0.93	2.55	3.048(15)	114
C(11)-H(11)···O(39)	0.93	2.45	3.262(16)	146

Table S4. Bond-valence sum (BVS) calculations of Cu, W and P for compound **1**.[a]

Atom	Oxidation states	Atom	Oxidation states
Cu1	1.82	Cu2	1.47
Cu3	1.87	Cu4	1.49
W1	6.15	W2	6.19
W3	6.35	W4	6.19
W5	6.25	W6	6.23
W7	6.19	W8	6.30
W9	6.35	W10	6.27
P1	4.72	P2	4.71

[a] The bond-valence sum (BVS) calculation method is according reference.[13]

Table S5. Selected bond lengths (Å) and bond angles (°) of compound **2**.

Cu(1)-N(2)	1.934(13)	Cu(1)-N(2^1)	1.934(13)	Cu(2)-N(7)	1.91(2)
Cu(2)-N(13)	2.151(12)	Cu(3)-Cl(1)	2.259(10)	Cu(3)-N(12)	1.936(12)
Cu(3)-N(12^1)	1.936(12)	Cu(4)-Cl(1)	2.585(4)	Cu(4)-N(16)	2.107(11)
Cu(4)-N(22)	1.87(2)	Cu(5)-N(14)	1.959(11)	Cu(5)-N(14^3)	1.958(11)
Cu(6)-N(8)	1.986(10)	Cu(6)-N(18)	1.993(10)	Cu(7)-Cl(2)	2.51(4)
Cu(7)-N(10)	2.05(2)	N(2)-Cu(1)-N(2^1)	133.6(6)	N(7)-Cu(2)-N(13)	101.5(7)
N(12)-Cu(3)-Cl(1)	113.7(3)	N(12^1)-Cu(3)-N(12)	131.0(6)	N(12^1)-Cu(3)-Cl(1)	113.7(3)
N(16)-Cu(4)-Cl(1)	105.3(4)	N(22)-Cu(4)-Cl(1)	147.7(7)	N(22)-Cu(4)-N(16)	106.6(7)
N(14^2)-Cu(5)-N(14)	127.4(5)	N(8)-Cu(6)-N(18)	141.9(5)	N(10)-Cu(7)-Cl(2^2)	111.1(14)
N(10)-Cu(7)-Cl(2)	95.7(11)	N(10^2)-Cu(7)-Cl(2^2)	95.7(11)	N(10^2)-Cu(7)-Cl(2)	111.1(14)

Symmetry transformations used to generate equivalent atoms: [1]+x,3/2-y,+z; [2]-x,1-y,1-z; [3]+x,1/2-y,+z; [4]1-x,1-y,2-z; [5]1-x,1-y,1-z.

Table S6. The hydrogen bond lengths (Å) and angles (°) of compound **2**.

Donor-H···Acceptor	D-H [Å]	H···A [Å]	D···A [Å]	D-H···A [°]
C(1)-H(1)···O(29)	0.95	2.518	3.093(12)	119.1
C(2)-H(2)···O(25)	0.95	2.59	3.52(2)	168
C(4)-H(4)···O(13)	0.951	2.555	3.087(13)	115.6
C(6)-H(6)···O(29)	0.95	2.408	3.041(12)	123.90
C(11)-H(11)···O(13)	0.95	2.39	3.34(2)	174.6
C(12)-H(12)···O(13)	0.95	2.418	3.014(11)	120.6
C(16)-H(16)···O(9)	0.95	2.353	3.286(13)	166.7
C(18)-H(18)···O(7)	0.951	2.233	3.176(12)	171.2
C(21)-H(21)···O(17)	0.95	2.360	3.284(16)	164.2
C(21)-H(21)···O(21)	0.95	2.593	3.260(14)	127.5
C(22)-H(22)···O(35)	0.950	2.572	3.506(15)	167.6
C(25)-H(25)···O(37)	0.950	2.348	3.254(17)	159.4
C(26)-H(26)···O(19)	0.950	2.418	3.359(15)	170.5
C(28)-H(28)···O(15)	0.95	2.25	3.17(2)	161
C(31)-H(31)···O(13)	0.95	2.57	3.15(3)	120
C(32)-H(32)···O(15)	0.949	2.324	3.014(14)	129.1
C(39)-H(39)···O(25)	0.95	2.591	3.539(19)	175

Table S7. Bond-valence sum (BVS) calculations of Cu, W and P for compound **2**.[a]

Atom	Oxidation states	Atom	Oxidation states
Cu1	1.14	Cu2	1.08
Cu3	1.14	Cu4	1.14
Cu5	1.15	Cu6	0.93
Cu7	1.10		
W1	6.24	W2	6.22
W3	6.32	W4	6.23
W5	6.14	W6	6.28
W7	6.26	W8	6.08
W9	6.19	W10	6.19
P1	4.72	P2	4.73

[a] The bond-valence sum (BVS) calculation method is according reference.[13]

Table S8. Comparison of compounds **1**–**2** with several reported catalysts on catalytic performance.

Catalysts	Time (h)	Temp. (℃)	Conv. (%)	TOF (h^{-1})	Reference
compound **1**	8	80	95	10.57	**This work**
compound **2**	8	80	92	12.14	**This work**
FeW–PYDC	24	100	95.7	13.29	14
$[Fe(H_2O)_3(dtb)][Fe(dtb)_2][HBW_{12}O_{40}]\cdot 12H_2O$	8	75	94	8,8	15
$(Hbiz)_{10}\{[Mn_{1.5}(\mu_2\text{-}O)_2(H_2O)_2][Mn(H_2O)_3]\{Mn[Mo_6O_{12}(OH)_3(H_2PO_4)(HPO_4)_3]_2\}\}_2\cdot 4H_2O$	24	60	95	8.8	16
HENU-7	24	75	96	8	17
$[Cu_4(\mu_2\text{-}OH)_4L_2][H_3PMo_{11}CuO_{40}]\cdot 12H_2O$	12	80	88	3.14	18
$Cu(II)/PMo_{12}$	10	90	93	3.1	19
$[Co_2(L)_{0.5}(MTC)(\mu_3\text{-}OH)(H_2O)_2]\cdot 2H_2O$	24	90	99	1.35	20
$[Cu^{II}(C_2N_2H_8)_2]_4[Cu^{II}(C_2N_2H_8)_2(H_2O)_2]_2[PNb_{12}O_{40}V^{V}V^{IV}O_2]\cdot(OH)_2\cdot 11H_2O$	24	60	95.8	1.25	21
$[Co^{III}(C_2N_2H_8)_3]_2[Co^{III}(C_2N_2H_8)_2(H_2O)_2]_{0.5}[H_{2.5}PNb_{12}O_{40}V^{V}V^{IV}O_2]\cdot 20H_2O$	24	60	93.4	1.21	21
$[Cu^{I}_2Cu^{II}(bix)_2]\{V_4O_{12}\}$	24	65	99	0.825	22
FZU-66-Co	16	R.T.	36.9	0.77	23
ZJU-18	65	18	18	0.2	24
Cu-MOF-SiF_6	36	60	28	0.07	25

Table S9. Crystal Data and Structural Refinement Details for $[Cu_3DTAB]Cl_3$.

Compound	$[Cu_3DTAB]Cl_3$
Formula	$C_5H_4Cl_{1.5}Cu_{1.5}N_3$
*M*r	254.60
Crystal system	monoclinic
Space group	$P2_1/m$
a [Å]	6.0636(5)
b [Å]	14.0476(10)
c [Å]	8.8949(7)
α, β, γ[°]	90, 14.0476(10), 90
V [Å^3]	733.17(10)
Z	4
Density (Mg/m^3)	2.307
Absorption coefficient (mm^{-1})	10.113
$F_{(000)}$	496.0
Cryst size(mm^3)	0.2 × 0.15 × 0.14
θ (deg)	10.278 - 134.246
Reflections collected	2371
Independent reflections	2371
GOF on F^2	1.113
Final *R* indices, R_1	0.0493
$wR_2[I>2\sigma(I)]$	0.1561
R indices, R_1	0.0502
wR_2(all data)	0.1573

Table S10. Selected bond lengths (Å) and bond angles (°) of $[Cu_3DTAB]Cl_3$.

Cu(1)-Cl(1)	2.3482(12)	Cu(1)-Cl(3)	2.6248(15)	Cu(1)-N(2^1)	2.004(3)
Cu(1)-N(3)	1.997(3)	Cu(2)-Cl(2)	2.109(2)	Cu(2)-Cl(3)	2.095(2)
Cl(1)-Cu(1)-Cl(3)	89.42(4)	Cl(1)-Cu(1)-N(2^1)	104.82(11)	Cl(3)-Cu(1)-N(2^1)	123.43(11)
N(3)-Cu(1)-Cl(1)	119.95(11)	N(3)-Cu(1)-Cl(3)	103.30(11)	N(3)-Cu(1)- N(2^1)	114.52(14)
Cl(3)-Cu(2)-Cl(2)	177.08(9)				

Symmetry transformations used to generate equivalent atoms: ^{1}-x,1-y,1-z; ^{2}+x,3/2-y,+z.

REFERENCES

1. W. Sun, B. An, B. Qi, T. Liu, M. Jin and C. Duan, Dual-excitation polyoxometalate-based frameworks for one-pot light-driven hydrogen evolution and oxidative dehydrogenation, *ACS Appl. Mater. Interfaces*, 2018, **10**, 13462-13469.
2. O. V. Dolomanov, L. J. Bourhis, R. J. Gildea, J. A. K. Howard and H. Puschmann, OLEX2: a complete structure solution, refinement and analysis program, *J. Appl. Crystallogr.*, 2009, **42**, 339-341.
3. L. J. Bourhis, O. V. Dolomanov, R. J. Gildea, J. A. K. Howard and H. Puschmann, The anatomy of a comprehensive constrained, restrained refinement program for the modern computing environment - Olex2 dissected, *Acta Crystallographica Section A*, 2015, **71**, 59-75.
4. G. Sheldrick, A short history of SHELX, *Acta Crystallographica Section A*, 2008, **64**, 112-122.
5. M. Frisch, Gaussian 09, Revision D. 01/Gaussian.*Journal*, 2009.
6. X.-X. Li, L. Zhang, J. Liu, L. Yuan, T. Wang, J.-Y. Wang, L.-Z. Dong, K. Huang and Y.-Q. Lan, Design of crystalline reduction–oxidation cluster-based catalysts for artificial photosynthesis, *JACS Au*, 2021, **1**, 1288-1295.
7. Z. Lang, J. Miao, H. Tan, Z. Su, Y. Li and Z. Zheng, Element table of TM-substituted polyoxotungstates for direct electrocatalytic reduction of nitric oxide to ammonia: a DFT guideline for experiments, *Inorg. Chem. Front.*, 2020, **7**, 4507-4516.
8. P. J. Hay and W. R. Wadt, Ab initio effective core potentials for molecular calculations. potentials for K to Au including the outermost core orbitals, *J. Chem. Phys.*, 1985, **82**, 299-310.
9. W. J. Hehre, R. Ditchfield and J. A. Pople, Self—consistent molecular orbital methods. XII. further extensions of gaussian—type basis sets for use in molecular orbital studies of organic molecules, *J. Chem. Phys.*, 1972, **56**, 2257-2261.
10. J. Tomasi, B. Mennucci and R. Cammi, Quantum mechanical continuum solvation models, *Chem. Rev.*, 2005, **105**, 2999-3094.
11. J. Gao, L. Gong, X. Fan, K. Yu, Z. Zheng and B. Zhou, $\{P_2W_{18}O_{62}\}$-encapsulated potassium-ion nanotubes intercalated in copper biimidazole frameworks for supercapacitors and hydrogen peroxide sensing, *ACS Appl. Nano Mater.*, 2020, **3**, 1497-1507.
12. M. C. Biesinger, L. W. M. Lau, A. R. Gerson and R. S. C. Smart, Resolving surface chemical states in XPS analysis of first row transition metals, oxides and hydroxides: Sc, Ti, V, Cu and Zn, *Appl. Surf. Sci.*, 2010, **257**, 887-898.
13. I. D. Brown and D. J. A. C. S. B. S. S. Altermatt, Bond-valence parameters obtained from a

systematic analysis of the inorganic crystal structure database, *Acta Cryst.*, 1985, **41**, 244-247.

14. Q. Wang, B. Xu, Y. Wang, H. Wang, X. Hu, P. Ma, J. Niu and J. Wang, Polyoxometalate-incorporated framework as a heterogeneous catalyst for selective oxidation of C–H bonds of alkylbenzenes, *Inorg. Chem.*, 2021, **60**, 7753-7761.
15. Y. Wang, Z.-X. Liu, X.-P. Zhao, Y.-Y. Ma, S.-M. Zhang, W.-J. Cui, J. Du and Z.-G. Han, Polyoxometalate-encapsulated metal-organic frameworks with diverse cages for the C–H bond oxidation of alkylbenzenes, *Chin. J. Struct. Chem.*, 2023, **42**, 100011.
16. X. Liu, N. Xu, X. Liu, Y. Guo and X. Wang, A new $\{P_4Mo_6\}$-based complex as a highly efficient heterogeneous catalyst for the oxidation of alkylbenzenes under mild conditions, *CrystEngComm*, 2024, **26**, 364-369.
17. B. Xu, Q. Xu, Q. Wang, Z. Liu, R. Zhao, D. Li, P. Ma, J. Wang and J. Niu, A copper-containing polyoxometalate-based metal–organic framework as an efficient catalyst for selective catalytic oxidation of alkylbenzenes, *Inorg. Chem.*, 2021, **60**, 4792-4799.
18. Y. Wang, Q. Liu, Y.-Y. Ma, Z.-X. Liu, Y.-N. Zhang, Y.-S. Wang, J. Du and Z.-G. Han, Polyoxometalate-embedded copper-organic network as dual-site synergetic catalyst for the selective oxidation of benzylic C−H bond, *Mol. Catal.*, 2024, **569**, 114579.
19. P. Li, Y. Wang, X. Wang, Y. Wang, Y. Liu, K. Huang, J. Hu, L. Duan, C. Hu and J. Liu, Selective Oxidation of Benzylic C–H Bonds Catalyzed by Cu(II)/$\{PMo_{12}\}$, *J. Org. Chem.*, 2020, **85**, 3101-3109.
20. Y.-Y. Li, X.-H. Li, N. Xu, Z.-X. An, Y. Chu and X.-L. Wang, A new metal−organic complex with coordination unsaturated Co(II) as high-efficiency heterogeneous catalyst for selective oxidation of alkylbenzenes, *Mol. Catal.*, 2023, **548**, 113428.
21. J. Hu, J. Dong, X. Huang, Y. Chi, Z. Lin, J. Li, S. Yang, H. Ma and C. Hu, Immobilization of Keggin polyoxovanadoniobate in crystalline solids to produce effective heterogeneous catalysts towards selective oxidation of benzyl-alkanes, *Dalton Trans.*, 2017, **46**, 8245-8251.
22. T.-Y. Dang, R.-H. Li, H.-R. Tian, W. Guan, Y. Lu and S.-X. Liu, Highly efficient multi-site synergistic catalysis of a polyoxovanadate-based metal–organic framework for benzylic C–H bond oxidation, *J. Mater. Chem. A*, 2022, **10**, 16514-16523.
23. K. Lin, J. Wang, S. Qiao and Z. Guo, Novel cobalt(II)-decorated 1D covalent organic framework for selective oxidation of ethylbenzene, *ACS Sustainable Chem. Eng.*, 2024, **12**, 6719-6727.
24. X.-L. Yang, M.-H. Xie, C. Zou, Y. He, B. Chen, M. O'Keeffe and C.-D. Wu, Porous metalloporphyrinic frameworks constructed from metal 5,10,15,20-tetrakis(3,5-biscarboxylphenyl)porphyrin for highly efficient and selective catalytic oxidation of alkylbenzenes, *J. Am. Chem. Soc.*, 2012, **134**, 10638-10645.
25. S. Wang, L. Li, J. Zhang, X. Yuan and C.-Y. Su, Anion-tuned sorption and catalytic properties of a soft metal–organic solid with polycatenated frameworks, *J. Mater. Chem.*, 2011, **21**, 7098-7104.